Evaluation of Simultaneous Dual-radioisotope SPECT Imaging Using ^{99m}Tc and ^{131}I

S. H. ALLehyani [1] (PhD), R. A. Hassan [1, 2] (PhD), B. S. Bahuwayrith [1] (MSc), S. M. Al-Qahtani [1] (PhD)

[1] Department of Physics, Faculty of Applied Sciences. Umm Al Qura University, Makkah, Saudi Arabia

[2] Department of Nuclear physics, National Cancer Institute, Cairo University, Cairo, Egypt

Abstract

The aim to study the effects of source concentration, acquisition & processing parameters on DSPECT image quality. The FWHM, differential uniformity, contrast, and SNR in the three transverse slices of the phantom was analyzed. When the phantom was filled with 20 mCi ^{99m}Tc & 0.4 mCi ^{131}I, were FWHM, differential uniformity and contrast are improved (*P*-values were statistically significant) with the higher SNR. On the other hand, HEGP collimator had better FWHM, differential uniformity and contrast with a suitable SNR. In the case of showed improvement of resolution in the case of 128 views rather than in 32 and 64 views. But in the case of Diff. Unif. % and the contrast we found that 64 NOP has the better values, which indicate the higher image quality. For SNR 32 NOP given the best values. In practice, approximately 60 views are adequate for most clinical studies. The scattering compensation is TEW subtraction method. Also, the study showed that, the reconstruction of DSPECT data were by (OSEM) iterative algorithm demonstrated quantitative accuracy comparable to FBP, FLASH-3D algorithm.

Key Words: *Simultaneous radioisotope, ^{131}I & ^{99m}Tc imaging, Dual Single Photon Emission Computed Tomography (DSPECT), Imaging factors, image quality.*

Introduction;

The routine use of dual radionuclide for nuclear medicine patient imaging can be complement by studies employing of two tracers of radionuclide to examine two different processes in a single organ, most frequently by simultaneous imaging of both radionuclides in different energy windows yielding perfectly registered image pairs of both radionuclide distributions [1] .Its advantages are to abbreviate the acquisition procedure with an identical geometrical registration of the different radionuclides images, with the same physiological condition without motion artifacts, and help patient throughput and comfort through imaging[2]. In nuclear medicine, simultaneous dual-isotope imaging can be used to diagnostic of some organs such as; ^{99m}Tc and ^{123}I for brain imaging [3], ^{99m}Tc and ^{201}Tl for cardiac imaging [4], ^{99m}Tc and ^{131}I for parathyroid imaging

[5], ^{99m}Tc and ^{123}I for renal imaging [6],[7]. Simultaneous dual-isotope imaging has potential in neurodegenerative diseases, e.g. Parkinson's disease, Huntington's disease and multiple-system atrophy [8]. Nakajima study evaluates dual-radionuclide with ^{99m}Tc and ^{111}In in simultaneous gastric emptying and bile transit study after gastric surgery [9].

Imaging by dual-isotope simultaneous acquisition techniques could reduce camera imaging time, the total time that a patient is in an imaging facility and errors induced by image misalignment. Simultaneously acquired dual-isotope rest ^{201}Tl/stress ^{99m}Tc -sestamibi studies are being evaluated for clinical use in some centers. Separate acquisition dual-isotope techniques have also been evaluated clinically [10]. Kelty et all described dual radionuclides imaging protocol using ^{99m}Tc labeled red blood cells with ^{111}In monoclonal antibody imaging for detecting and localizing nodal metastasis in prostates cancer. They conclude that the dual radionuclides technique assures the precise image registration needed for accurate comparison of blood pool and pelvic lymph node activity that is required for confident and accurate image interpretation [11]. Yamada suggests that the feasibility of the novel Cadmium zinc telluride-based scanner for the simultaneous ^{99m}Tc-tetrofosmin /^{123}I-BMIPP (beta methyl iodophenyl pentadecanoic acid) dual-tracer acquisitions in clinical settings [12].

The gamma camera heads rotate around the patient in circular, elliptical or body contour orbits to acquire the projection. The flexibility of the different motions that are available in modern gamma camera SPECT systems allow the gantry to move in orbit, similar to body contour, resulting in improved spatial resolution. [13, 14] The projection profile is a discrete function, acquiring the data at a finite number of angular sampling intervals around the object. Ideally, for accurate reconstruction, the number of angular views over a full 360° arc should be equal to a projection matrix size between 64 and 128 for FOV, and a 180° arc should be between 64 and 32 projection views. For each angular position, each point of the detector contains a number of recorded counts or scintillations which are proportional to radionuclide concentration at same point on the object. [14]

Modern SPECT system designs increase the number of Gamma camera heads so that multiple views can be acquired simultaneously in the same acquisition. Dual-detector head systems currently predominate [15]. The selection of the appropriate collimator for an isotope is necessary by considering the photo peak energy and scattering photons not included in the image. For example, the isotope ^{123}I has the main γ photo-peak at 159 keV and there are a number of high-energy photons that can penetrate through or maybe scatter in the collimator septa. The Medium-Energy low-penetration collimator performed well with I-123 energy gamma photons, but the low resolution makes it unsuitable to use for acquisition in small structures such as parathyroid [16]. The High-energy (HE) collimators is the best collimator for ^{131}I imaging, but medium-energy (ME) collimators is applicable for ^{131}I imaging not only whole-body imaging but also in SPECT imaging [17].

The attenuation of overlying tissue is the largest factor, which produce both a loss of quantitative accuracy and artefacts in the resulting SPECT images. Concerning the nature of materials, attenuation will vary with

the materials traversed, even if the thickness between the site of emission and the detector is the same. In other words, there is a difference if the photons pass through muscle, lung or bone. Thus, patient-specific information is needed on the spatial distribution of attenuation coefficients to calculate the attenuation that occurs when photons are emitted from a given location in the patient and then detected at the detector. This is called the attenuation map, which is fundamental to perform attenuation compensation [14, 18]. Most of photons emitted from the radionuclide experience Compton or coherent scatter in the patient at least once before exiting the body; some of the scattered photons may pass through the collimator and be detected. In most studies, scattered photons account for 30 to 40% of the photons detected in the photo-peak energy window of a SPECT gamma camera system [19].

There are many proposed approaching for the correction of scatter, including direct measurement, modelling, or some combination of both [19]. One more recent scatter correction method involves using a triple-energy window (TEW) technique, uses the photo-peak window and relies on two narrow energy windows, one of higher and one of lower energy [20]. It involves subtraction of the scatter estimates, pixel by pixel, from the photo-peak projection images. This approach is suitable for situations where there is down scatter from the higher-energy emissions, as well as scattering from the identified photo-peak emissions [19].

One major complication in simultaneous dual-radionuclide imaging arises with cross-talk effects caused by down scattering from the higher-energy emissions detected in the lower-energy photo-peak. The phenomenon refers to the presence of Compton-scattered photons from one isotope in the primary energy window of a second isotope. The down scatter, unlike scatter in the photo-peak, is the result of higher-order scatter, which can be difficult to estimate. So, it is necessary to develop a method to correct for this cross-talk. Several cross-talk compensation approaches have been developed to make the simultaneous dual-radioisotope protocols clinically feasible. Multiple energy windows can be used for dual-radionuclide imaging by estimating scatter in each photo-peak energy window based on the projection data acquired on other photo-peak windows [21].

Noise is a fundamental problem in nuclear medicine imaging, but it presents a much greater problem for SPECT imaging than for planar imaging. The main reason is that the noise in images results from statistical variations in the number of the emitted photons counted in a given counting interval due to the random nature of radiation decay and interactions with the patient and camera system [13, 22]. In practice, SPECT ideal result is not achieved because the projection data are degraded by many factors, including physical, instrumentational, patient, organ and radiopharmaceutical factors [23].

The aim of reconstruction is to generate a 2-D cross-sectional image of the activity distribution for a 3-D object. Reconstruction of the image has two approaches: filtered back projection (analytical reconstruction) and iterative reconstruction.[24]

Filtered back projection is an analytical method that is the most widely used in clinical SPECT systems, because of its speed, simplicity, and computational efficiency. It consists of two steps: filtering of data and back projection of that filtered data [25].

Iterative reconstruction starts with an initial estimate of the image. [26] Most of the times the initial estimate image is very simple, for example a uniform activity distribution. Then a set of projection data is estimated from the initial estimate using a mathematical process called forward projection. The resulting projections are compared with the recorded projections and the differences between them are used to update the estimated image. The iterative process is repeated many times until the differences between the calculated and measured data are smaller than a specified preselected value. The iterative reconstruction methods include statistical algorithms like maximum likelihood expectation maximization (MLEM), algebraic methods like the algebraic reconstruction technique (ART) and ordered subsets expectation maximization (OSEM) [27].

The main purpose of this work studying the effects of radioactive sources concentrations ratio and some acquisition & processing parameters on DSPECT image quality.

Materials and methods

i-Phantom Preparation;

To simulate the patients imaging, a commercially available, dedicated, compartment striatal phantom (Flangeless Deluxe Jaszczak phantom) used for all our studies. This tissue-equivalent Jaszczak phantom consists of a cylinder inside has Insert and spheres, cold spheres (CS), resolution rods (RR), and the remainder of the cylinder as one compartment. The phantom was filled with radionuclide solutions (^{99m}Tc& ^{131}I) to simulate the accumulation of ^{99m}Tc and ^{131}I in the human body. The phantom was constructed of a clear Acrylic Plexiglass material and consists of cylinder inside diameter: 20.4 cm, cylinder wall thickness: 6.4 mm, cylinder inside height: 18.6 cm, with six spheres. Height of center of spheres from base plate: 12.7 cm, spheres with different diameters (9.5, 12.7, 15.9, 19.1, 25.4, and 31.8 mm) and rods with height of: 8.8 cm, their are148 rods (4.8, 6.4, 7.9, 9.5, 11.1, and 12.7 mm). An approximately 30 mm cylindrical hole located in the upper to measure the image resolution, we performed a phantom study to evaluate the quality of the Dual SPECT images. Figure (1) shown that the phantom was used in our experimental acquisition.
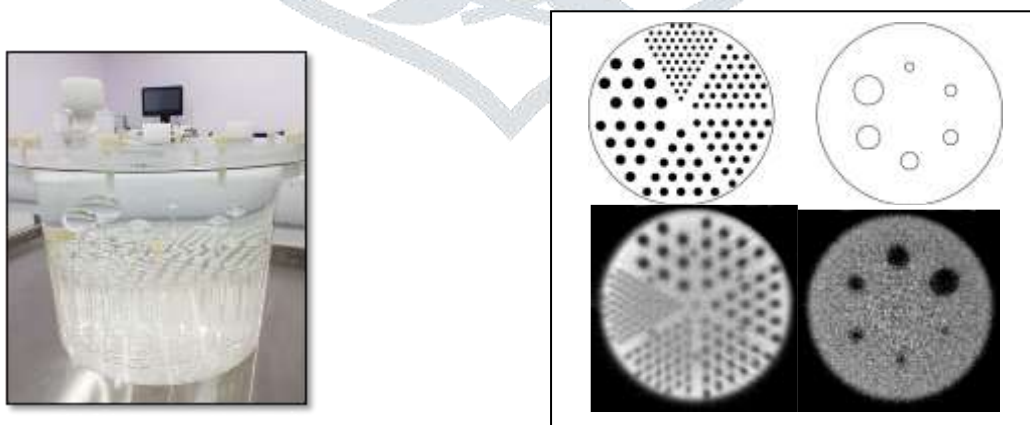

Figure1. Deluxe Jaszczak phantom

ii- Imaging Techniques;

All experimental data in this investigation were acquired with a dual-head, rotating camera dedicated to SPECT/CT (Symbia gamma camera from Siemens, at Al-Hada Military hospital) with high energy collimator, as shown in figure (2). The SPECT scanner system was equipped with a dual-head gamma camera with 9.5-mm-thick NaI crystals, had a 38.7 9 53.3 cm FOV, and was combined with a spiral 6-slice CT in the same gantry [24].

Dual radioisotopes used in this investigation were ^{99m}Tc and ^{131}I, were injected into the phantom to be imaged simultaneously by the gamma-camera. In this case we were studied the different physical parameters effecting the DSPECT images quality. Separate radionuclide measurements were performed by acquiring the data for Deluxe phantom, which is prepared as follow: (1) We fill the phantom by water and is injected by ^{99m}Tc and 0.4 mCi of ^{131}I. Then we shake the phantom to be a good uniform distribution of Dual radioisotopes.

(2) Mount the phantom on the end of the table, which is adjusted to be as close as possible or parallel to the axis-of-rotation so that both the detectors and the phantom must be in the same level. (3) High-energy, all-purpose, parallel-hole collimator (HEGP) or Medium-energy, all-purpose, parallel-hole collimator (MEGP) was used on each detector. (4) We set the acquisition matrix to the 128×128, the number of views 64 views over 180° and 1.23 zoom factor that will give a pixel size is 3.9 mm. (5) Data acquired in 30 sec for each projection. (6) The images were reconstructed by iterative (OSEM) algorithm, with 30 iterations and 2 subsets. (7) The scatter and attenuation correction where be applied. Figure 3 show transverse reconstructed Image of phantom of dual 30 mCi of ^{99m}Tc with 0.4 mCi ^{131}I (left) and only 5 mCi ^{99m}Tc, with 0.4 mCi ^{131}I (right)**.**

In our study we evaluate the effects Source Activities concentration, Collimator type (HEGP vs MEGP), and effects of Number of projections (32,64 vs 128) Data acquired in 15, or 30 or 60 sec for each projection. The quality of the constructed images was studied by evaluation the resolution, contrast, SNR and uniformity for each situations of our study.


Figure 2. Symbia gamma camera from Siemens
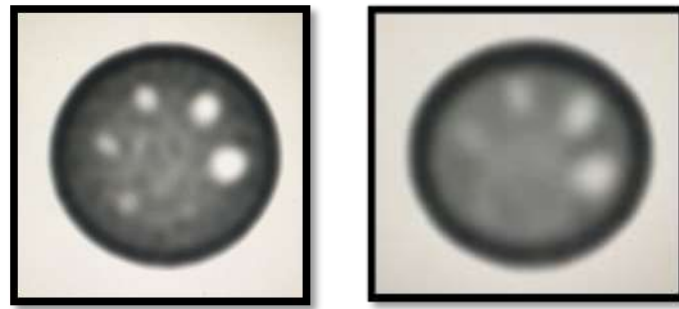
Figure 3. Transverse reconstructed Image of phantom of dual 30 mCi of ^{99m}Tc with 0.4 mCi ^{131}I (left) and only 5 mCi ^{99m}Tc, with 0.4 mCi ^{131}I (right)

iii-Data analysis;

(1) **Contrast**; A definition of contrast refers to the ratio of signal change for an imaged object, such as a lesion, relative to the signal level of areas that surrounding the imaged object. The contrast can be measured from equation:

$$C_I = \frac{R_l - R_\circ}{R_l} \qquad (1)$$

Where R_l the count is rate over surrounding tissue, and $R_\circ$ is the count rate over a ROI or lesion. The contrast can be calculated by following steps: 1- we display the entire set of data and select the three transverse sections (3 TV) where the cold spheres are most clearly defined. (Note that the number of spheres must be visualized). 2- Draw a circle ROI on largest spheres in the chosen slice and other circle in the background (uniform section of the phantom). 3- Determine the number of counts in the sphere (cold sphere) and the count in the background. Then we can calculate the contrast from above equation.

(2) **Reconstructed image uniformity (U);** Quantitative assessment of image uniformity involves a change in pixel counts in small regions of interest across the FOV (Diff. Uniformity). However, the simple metrics of non-uniformity do not provide a complete assessment of what the eye perceives in the assessment image. Thus, visual analysis is also very important. Diff. Uniformity for a given three uniform transverse slices, was defined as the average of five uniformity measurements, which made on five background ROIs. Here, each uniformity measurement for a given ROI was defined as the mean counts per voxel within the ROI (normalized to its maximum value).

The uniformity can be measured by taking the ratio of subtraction to the addition of maximum and minimum counts of any five consecutive pixels across rows or columns of the image's slice.

$$\text{Diff. Uniformity (\%)} = \frac{max.pixel\ count - min.pixel\ count}{max.pixel\ count + min.pixel\ count} \times 100 \qquad (2)$$

The image uniformity can be calculated in following steps:1- Select three uniform slices (no cold sphere or rods visualized). 2- draw a 5 pixels-wide horizontal line region-of-interest (ROI) centered on the images. 3- Record the mean counts per pixel, the maximum and minimum pixel counts within ROI. 4- Calculate the reconstructed image Diff. uniformity by the equation (2).

(3) **Resolution of hot and cold sphere of phantom;** The resolution was measured by the full width at half maximum (FWHM), Spatial tomographic resolution (in mm) obtained by the drawing an approximately 5-mm region of interest (ROI) around cylindrical hole which located in the upper center of the phantom. The ROI was the same size as the hole in the phantoms. (4) SNR; (Signal to noise ratio) for a given image, was defined as the average of five voxels measurements made on the five independent background ROIs. Specifically, the SNR for a given background ROI was defined as ratio of the mean counts per voxel within the ROI   to its standard deviation;

$$SNR = \frac{mean\ pixel\ value}{standard\ deviation} \qquad (3)$$

we defined the average of three SNR measurements made on the three independent background ROIs.

The image SNR can be calculated in following steps: 1- display the entire data set of reconstructed images that has uniform slices.2- Draw a circle as a (ROI) and record the mean count per pixel and the standard deviation.3- Calculate the SNR from the equation (3).

i. Source Activities concentration;

First, we studied the effect of different activities concentration of isotopes used on the quality of dual SPECT imaging. The DSPECT acquisition was performed by using a phantom which filled with water containing different activities concentration of ^{99m}Tc   (5 mCi, 10 mCi, 15 mCi, 20 mCi, 20 mCi, 25 mCi and 30 mCi) and 0.4 mCi of ^{131}I as in table 1, which are imaged simultaneously for each concentration. Then we position the Jaszczak phantom on the end of the SPECT table as discussed earlier.

The qualities of the reconstructed images were compared in terms of image contrast, SNR, uniformity and spatial resolution.

Table 1. The comparing of different activities ^{99m}Tc with 0.4 mCi of ^{131}I.

	Tc-99m activity (mCi)	I-131 activity (mCi)
1	5 mCi	0.4 mCi
2	10 mCi	0.4 mCi
3	15 mCi	0.4 mCi
4	20 mCi	0.4 mCi
5	25 mCi	0.4 mCi
6	30 mCi	0.4 mCi

ii. Collimator type (HEGP vs MEGP)

Variations in collimator geometry cause differences in the effect of quality of DSPECT imaging. The choice of Gamma camera collimator is suggested to play a critical role in determining the quality of gamma camera imaging in both planar and SPECT. In this study the we compare between two parallel hole collimators were used: high-energy, low-resolution collimator (HEGP) and medium-energy collimator (MEGP) for the best result activity concentration of ^{99m}Tc which was 25mCi with 0.4 mCi of iodine as in table 2. The phantom of activity of 25mCi of ^{99m}Tc with 0.4 mCi of ^{131}I was prepared as discussed earlier, then imaged simultaneously for each collimator type (HEGP & MEGP).We set the same acquisition parameters matrix to 128×128, the number of views to 64 views over 180° and 1.23 zoom factor that will give a pixel size is 3.9 mm. Data acquired in 30 sec for each projection. The images were reconstructed by iterative (OSEM) algorithm, with 30 iterations and 2 subsets. The scatter and attenuation correction where be applied.

Table 2. The comparison between 2 type of collimator for the best concentration or radionuclide used.

	I-131 activity (mCi)	Tc-99m activity (mCi)	Collimator type
1	25	0.4	HEGP
2	25	0.4	MEGP

iii. Number of projections (32,64 and 128)

The number of projections is essential for quantitative assessment. varying number of projections and Time per projection, allows effecting the image accuracy. In this study the we compare between three Number of projections (32,64 & 128) for the best result activity concentration of ^{99m}Tc which was 25mCi with 0.4 mCi of iodine as in table 3. The phantom of activity of 25mCi of ^{99m}Tc with 0.4 mCi of ^{131}I was prepared as discussed earlier, then imaged simultaneously for each number of projections (32,64 & 128).We set the same acquisition parameters matrix to 128×128, and 1.23 zoom factor that will give a pixel size is 3.9 mm. Data acquired in 60 sec, 30, 15 sec for each number of projection respectively. The images were reconstructed by iterative (OSEM) algorithm, with 30 iterations and 2 subsets. The scatter and attenuation correction where be applied.

Table 3. The comparison of 3 types of number of projections 32, 64 &128 views.

	I-131 activity (mCi)	Tc-99m activity (mCi)	No. of projection	Time per projection
1	25	0.4	32	60 sec
2	25	0.4	64	32 sec
3	25	0.4	128	15 sec

iv. Scattering correction

Since the scatter spectrum cannot be measured experimentally, the scatter fraction in the photopeak from the counts acquired can be estimated by using the TEW approach in two adjacent narrow windows. At each pixel, the scattered photons are estimated and then subtracted from the total counts measured in the photopeak to reject the unscattered photons.

We applied TEW correction for 99m Tc and ^{131}I. When we have applied the TEW correction for 99m Tc the higher sub-window can be ignored because the spectrum tends to zero above the photopeak. And the main window width was140 keV which set at 20% and sub-window was at 20% of the main window. Moreover, we applied two sub-windows (upper and lower) set at 20 % adjacent to main ^{131}I window with width 364 keV, which was set at 15 % [29,32].

All projection data acquired at the same acquiring parameters (128X128) pixel size, 1.23 zoom, 64 views, non-circular orbit, time 30 sec per view), for the best concentrations of 99m Tc versus 400 µCi of ^{131}I HEC. The reconstruction method was OSEM iterative algorithm. The compression was between scatter corrected and uncorrected image, Where the uncorrected images were acquired by ignoring the correction sub-windows.

v. Different reconstruction methods

Table 4 compares the two different algorithms of reconstruction the data that acquired simultaneously in the standard acquiring parameters (128X128) pixel size, 1.23 zoom, 64 views, non-circular orbit, time 30 sec), for all concentrations of 99m Tc with 0.4 mCi of ^{131}I. The projection data were reconstructed by either FBP with different filters or iterative (OSEM) algorithm. These tests were performed that compared with ideal reconstruction method, which is called; Flash 3-D. First, we were applying the (OSEM) iterative reconstruction method on the acquiring data. The image reconstruction was carried out using an ordered subset-expectation maximization (OSEM) method with 16 iterations and two subsets.

Table 4: The comparing of different reconstruction methods.

	^{131}I activity	^{99m}Tc activity	Reconstruction method
1	0.4 mCi	Best concentration	(OSEM) Iterative
2	0.4 mCi	Best concentration	Flash 3-D
3	0.4 mCi	Best concentration	FBP (Butterworth, winner, Metz)

In other situation, the same acquiring data as in the first situation were reconstructed using FBP algorithm. The reconstruction methods were repeated three times by varying the filters, which are (Butterworth, winner, Metz) filter. In each time the reconstruction was made by the filter which we selected and with cut-off about 0.55. Then the processing was for each situation of theses to evaluate the image quality, which was compared to the ideal reconstruction method (Flash-3D), which performed at the third situation.

Results & Discussion

i. Source Activities concentration

From study using the Jaszczak phantom we got four quantitative measurements and statistical information, when the reconstructed slices were analyzed. All the quantitative measurements were taken on the transverse slices. The first quantitative measurements were the full width at half maximum (FWHM) of the three transverse slices, where it expresses the regional resolution in the area of interest. The second quantitative measurement was the uniformity of the slices, the third measurement was the contrast, and the fourth is signal to noise ratio (SNR).

Spatial resolution quantifies size of the smallest object that can be determined reliably and often expressed as the full width at half-maximum (FWHM) of a point spread function. For projection data acquired with our system. We have found that the FWHM, differential uniformity, contrast, and signal to noise ratio values were affected much in DSPECT by varying the Source Activities concentration in the same acquisition parameters sets we have used. In table (5) we calculated image quality parameters. It's well known that the FWHM, differential uniformity, contrast, and signal to noise ratio values improved by increasing the ^{99m}Tc activity and vice versa, but this improvement will definite, from the table the changes in the values of the image quality parameters are statistically significant (P <0.05). Figure 4 show the best quality of reconstructed image of dual ^{99m}Tc/^{131}I with 20 mCi of ^{99m}Tc concentration, compared to other ^{99m}Tc concentration in the phantom, which have the pest resolution (FWHM= 20.61±1.77). While figure 5, 6, and 7 illustrate separate relations of the Source Activities concentration on the other image quality parameters (uniformity, contrast, and SNR).

The maximum uniformity improvement was with 20 mCi of ^{99m}Tc concentration for the Diff. uniformity in case of the Source Activities concentration set DSPECT 20mCi ^{99m}Tc, and the minimum percent was 3.481±0.94 for acquisition Source Activities concentration set DSPECT 10mCi ^{99m}Tc. Figure (5) showed the change of percent uniformity for different DSPECT Activities concentration.

Reconstructed tomographic contrast & SNR of all experiment DSPECT images of the phantom obtained were shown in table 5 & Figure (6,7). The calculated contrasts of the concentrations 5, 10, 15, 20, 25 ,30 mCi of ^{99m}Tc were 0.422±0.01, 0.338±0.049, 0.320±0.027, 0.506±0.02, 0.473±0.043, 0.326±0.030, respectively, P= 0.0015 and the calculated SNR were 29.737±2.87, 50.784±2.65, 34.154±2.18, 50.27±1.85, 45.181±1.64, & 47.53±2.22, respectively, P= 0.0146, the best calculated contrast were 0.506±0.02 of DSPECT 20mCi ^{99m}Tc,

for SNR of the different concentrations of experimental phantom images from reconstructed DSPECT were shown in Table 1. From table 1 it is evident that best reconstructed SNR is nearly equal to 50.784±2.65 for DSPECT 10mCi ^{99m} Tc, but for our interest DSPECT 20mCi ^{99m} Tc about 50.27±1.85, but we found that the other best image quality parameters of reconstructed image (FWHM, Diff. Unif. %, Contrast) of dual ^{99m} Tc/^{131}I activities concentration are for DSPECT 20mCi ^{99m} Tc. So, we were choosing this Activities concentration to have the best image quality.

Table 5. The relation between Source Activities concentration of DSPECT & quality parameters of reconstructed image (FWHM, Diff. Unif. %, Contrast, and SNR).

Parameters	FWHM	Diff. Unif. %	Contrast	SNR
DSPECT 5mCi Tc	26.45±2.43	3.762±0.25	0.422±0.01	29.737±2.87
DSPECT 10mCi Tc	23.07±1.65	3.481±0.94	0.338±0.049	50.784±2.65
DSPECT 15mCi Tc	21.96±1.27	3.405±0.15	0.320±0.027	34.154±2.18
DSPECT 20mCi Tc	20.61±1.77	2.150±0.92	0.506±0.02	50.27±1.85
DSPECT 25mCi Tc	22.47±1.74	3.337±0.12	0.473±0.043	45.181±1.64
DSPECT 30mCi Tc	23.84±2.39	2.131±0.19	0.326±0.03	47.53±2.22
P value	0.0198	0.0699	0.0015	0.0146
P<0.05 is defined to be significant				

Figure 4. Relation between Source Activities concentration of DSPECT & FWHM.
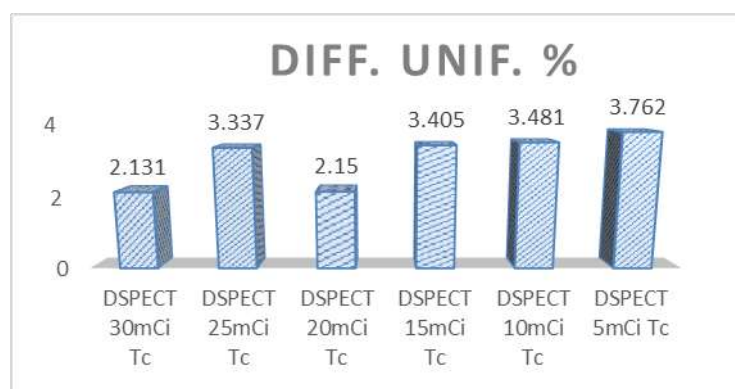

Figure 5. Relation between Source Activities concentration of DSPECT & DIFF. UNIF. %
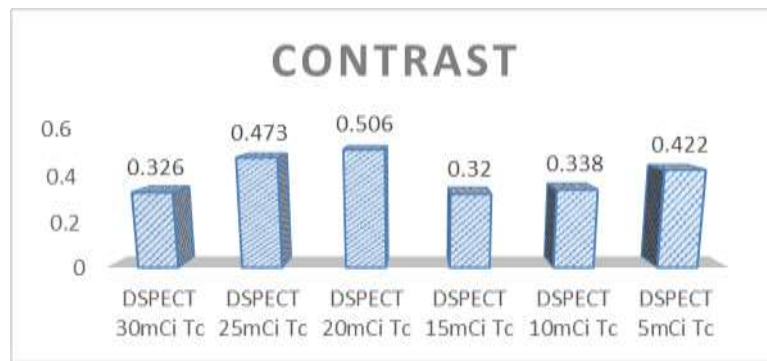
Figure 6. Relation between Source Activities concentration of DSPECT & contrast.
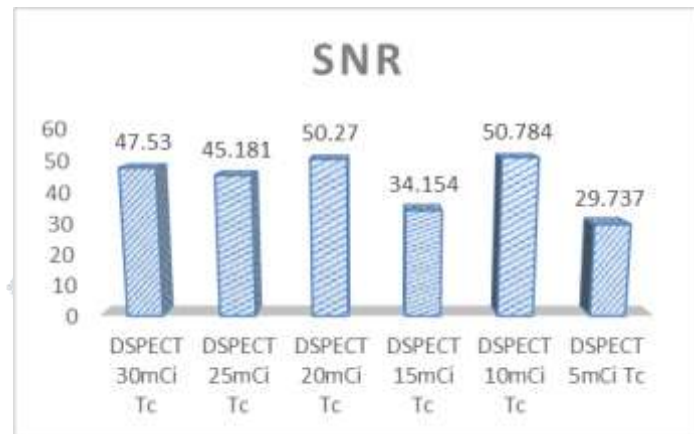
Figure 7. Relation between Source Activities concentration of DSPECT & SNR.

ii. Collimator type (HEGP vs MEGP)

DSPECT image reconstruction requires that the incident directions of each acquired count must be known. An external collimator is used to do so, by absorbing of photons which outside a range of incident angles as specified by the collimator designs. By limiting the number of detected photons to a specific direction, the collimator allows the detection of only a very small fractions of the photons emitted by the patient. The selection of which collimator to use is important to resultant DSPECT image quality. The results as in table 6 & figures 8 -11 revealed that changing type of collimator affect quality of DSPECT images. The value of the FWHM was improved for the HEGP, compared to MEGP value. 21.53±1.43 & 24.91±2.01 respectively. On the other hand, we get improving values of Differential uniformity for HEGP collimator (2.709±1.56), and also increasing the image contrast (0.528±0.03), but we found that increasing SNR for MEGP than HEGP collimator, this may be due to the reduction in total counts with HEGP can increase the image noise. However, this decreasing of counts can be improved by other parameters of study as increasing the number of views; it must be taking into consideration the whole time of acquisition to be suitable for patient stability during imaging.

Table 6.The relation between collimator type of DSPECT & quality parameters of reconstructed image (FWHM, Diff. Unif. %, Contrast, and SNR).

Parameters	FWHM	Diff. Unif. %	Contrast	SNR
DSPECT 20 mCi Tc MEGP	24.91±2.01	3.468±1.81	0.3362±0.01	56.023±1.91
DSPECT 20 mCi Tc HEGP	21.53±1.43	2.709±1.56	0.528±0.03	49.118±2.18
P value	0.0118	0.0112	0.0006	0.0182
P<0.05 is defined to be significant				
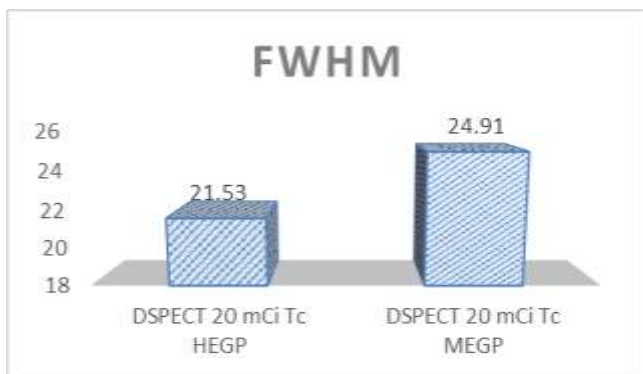
Figure8. Relation between collimator type of

DSPECT & FWHM
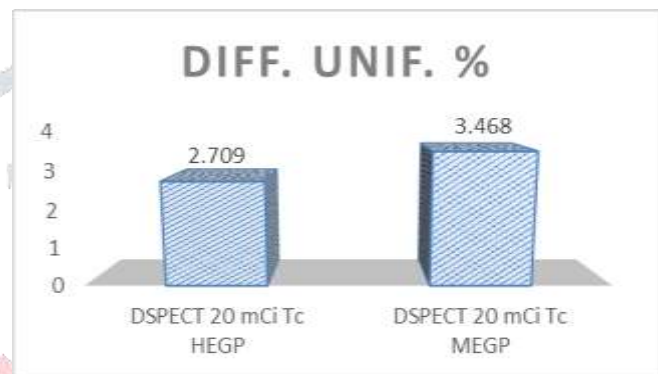
Figure9. Relation between collimator type of

DSPECT & DIFF.UNIF%

Figure 10. Relation between collimator type of
DSPECT & contrast.

Figure 11. Relation between collimator type of
DSPECT & SNR

iii. Number of projections (NPP) 32 vs 64, 128 views withTime per projection (TPP) 60 sec vs 30,15 sec.

We know that Increasing the number of projections (views) leads to the best definition of the SPECT images quality. So, the data represented in Table. 7., and Fig. 12, -15 showed improvement of resolution (FWHM) in the case of 128 views 20.81±0.024 rather than in 32 and 64 views. But in the case of Diff. Unif. % and the

contrast we found that 64 NOP (number of projections) has 2.4673 ± 0.008, 0.5273±0.043 respectively. Which indicate the higher image quality. For SNR 32 NOP given 52.35±0.635 the bet values. From the previous factors, we can decide that 64 NOP gives the best image quality. In practice, approximately 60 views are adequate for most clinical studies.

Table 7. The relation between number of projections of DSPECT & quality parameters of reconstructed image (FWHM, Diff. Unif. %, Contrast, and SNR).

Parameters	FWHM	Diff. Unif. %	Contrast	SNR
DSPECT,NOP=32/TPP=60sec	26.45±0.125	3.7630 ± 0.03	0.3383±0.01	52.35±0.635
DSPECT,NOP=64/TPP=30sec	21.74±0.445	2.4673 ± 0.008	0.5273±0.043	50.72±0.928
DSPECT,NOP=128/TPP=15sec	20.81±0.024	2.9938 ± 0.0265	0.5061±0.02	49.307±1.2
P value	0.0463	0.0311	0.0215	0.0365
P<0.05 is defined to be significant				

Figure 12. Relation between number of projections of DSPECT & FWHM.
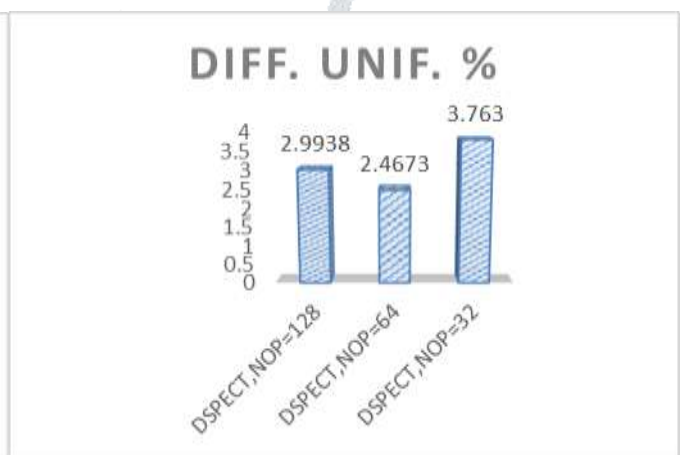

Figure 13. Relation between number of projections of DSPECT & DIFF. UNIF.%
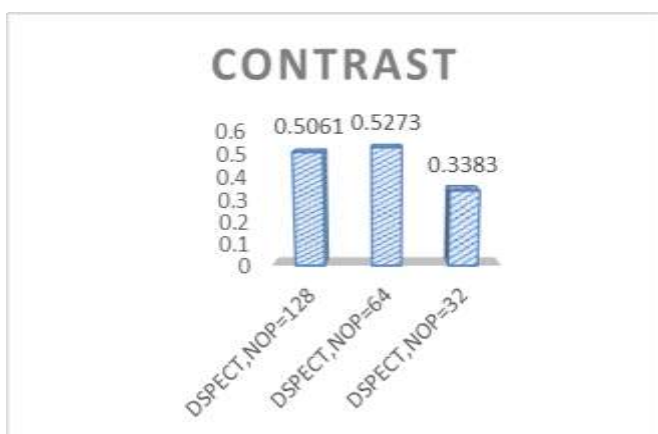
Figure 14. Relation between number of projections of DSPECT & contrast.

Figure 15. Relation between number of projections of DSPECT & SNR.

iv. Scatter correction

In DSPECT study, it is important to eliminate the scattered photons from the reconstructed image. In this study, the triple energy window (TEW) method, which has used to eliminate the scattered counts in measured counts, was applied to ^{99m}Tc / ^{131}I SPECT image. We assumed their photopeak energies to be 141 and 364 keV for ^{99m}Tc / ^{131}I respectively. Table (8) show that the relation between scatter corrected and uncorrected image with 20 mCi of ^{99m}Tc and 0.4 mCi of ^{131}I, and image quality parameters. Quantitative analysis done by using a FWHM, Diff. Unif. %, Contrast and SNR.

Although the counting rate were lost by applying the scatter correction of the DSPECT image due to the subtraction of the scatter image, it had improved the contrast (0.563335±0.094) & FWHM (23.81± 0.157). Improvements in Diff. Unif. % could be seen on the scatter corrected values, which was (1.467311± 0.086). From these results, the corrected images obtained with the triple energy window methods gave good agreement with the ideal images reconstructed from the projection data of primary photons.

Figures 16 and 17 shows that the image FWHM (23.81± 0.157) and Diff. Unif. % (1.47± 0.086) which improved for scattering corrected than uncorrected image.

Figures 18 and 19 shows that the image contrast and SNR (0.563335±0.094) and (51.667±0.056) which much improved in the corrected DSPECT 20mCi ^{99m}Tc and 0.4 mCi of ^{131}I image. For the scatter correction, there is the expected result that the image becomes less "noisy" as the count density increases.

Table 8: The relation between scatter corrected/uncorrected DSPECT image & quality parameters of reconstructed image (FWHM, Diff. Unif. %, Contrast, and SNR).

Parameters	FWHM	Diff. Unif. %	Contrast	SNR
DSPECT 20mCi Tc (with SC)	23.81± 0.157	1.467311± 0.086	0.563335±0.094	51.667±0.056
DSPECT 20 mCi Tc (NO SC)	26.27± 0.341	2.59366± 0.299	0.506158± 0.058	39.2±0.098
P value	0.0245	0.0178	0.0465	0.0468
P<0.05 is defined to be significant				
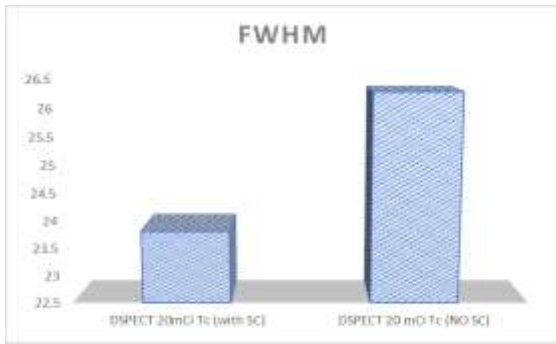
Figure 16: Relation between scattering & FWHM.
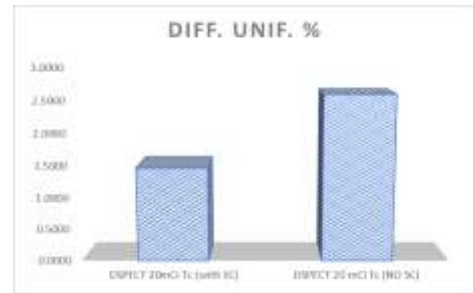
Figure 17: Relation between scattering & Diff. Unif. %.
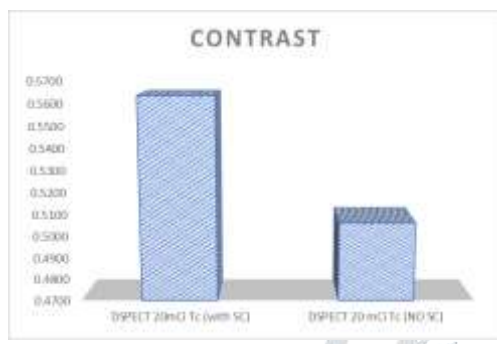
Figure 18: Relation between scattering & contrast.
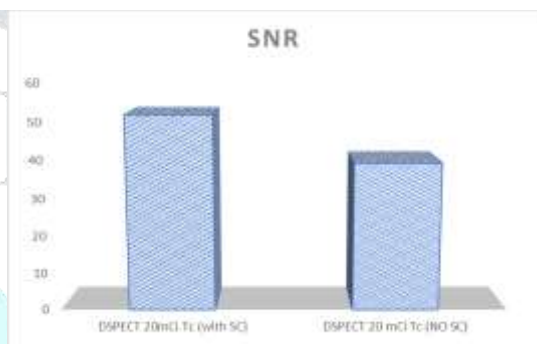

Figure 19: Relation between scattering & SNR.

v. R

The DSPECT image quality for (20 mCi 99m Tc and 0.4 mCi 131I) using HEGP, 64 projections which acquired at 30 sec per projection, were reconstructed by three different algorithms, as shown in table 9. The different algorithms were: iterative (OSEM), iterative (Flash-3D) and FBP with three different filters (Butterworth, Winner and Metz).

Table (9) presents the comparison between 5 classes of reconstruction methods, showed the improvement in FWHM, Contrast, Diff. Uniformity % and SNR for (OSEM) iterative reconstruction methods compared to FLASH 3-D and FBP (if no additional filter was applied). For OSEM iterative algorithm (30 iterations and 2 subsets) the measurements were 23.81, 1.46, 0.506 and 45.405 for FWHM, contrast, Diff. Uniformity % and SNR, respectively. All data are represented in Figures 20 to 23. For different types of filters which was applied on FBP we found that the best FWHM and SNR for Butterworth Filter were 25.71, 42.74 respectively. The best contrast and Diff. Uniformity % were for Metz Filter 0.49 and 2.43 respectively. The best contrast and Diff. Uniformity % were for Metz Filter 0.49 and 2.43 respectively.

Table 9: The comparison between different reconstruction methods for 20 mCi ^{99m}Tc and 0.4 mCi ^{131}I.

| Parameters	FWHM	Diff. Unif.	Contrast	SNR
Iterative (OSEM) algorithm 30 iterations, 2 subsets	23.81 ± 1.35	1.467 ± 0.054	0.506 ± 0.045	45.4059 ± 1.64
Iterative (Flash-3D) algorithm	27.61 ± 0.93	3.634 ± 0.16	0.483 ± 0.063	21.912 ± 2.03
FBP (Butterworth Filter)	25.71 ± 0.65	3.554 ± 0.43	0.430 ± 0.074	42.74 ± 1.94
FBP (Winner Filter)	29.47 ± 1.09	3.215 ± 0.096	0.458 ± 0.083	21.759 ± 0.95
FBP (Metz Filter)	28.85 ± 0.69	2.434 ± 019	0.490 ± 0.042	35.783 ± 1.42
P value	0.0443	0.0371	0.0251	0.0438
P<0.05 is defined to be significant				
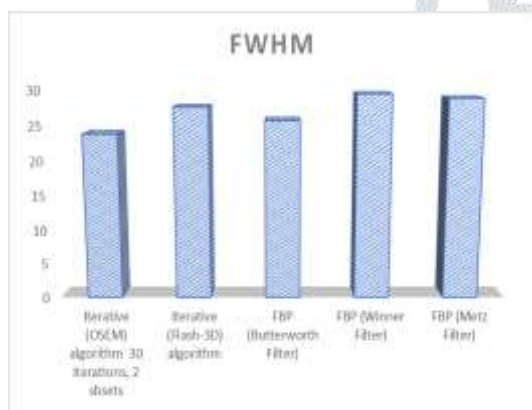
Figure 20: Relation between reconstruction

methods & FWHM.
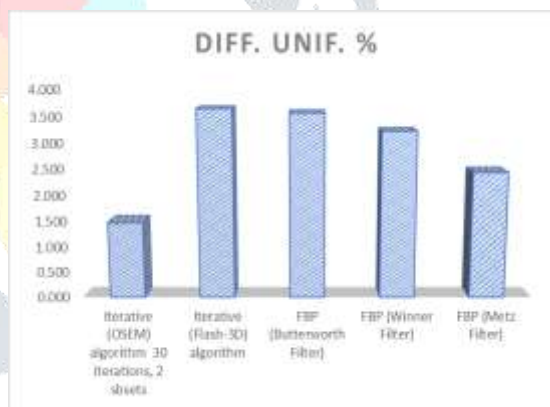
Figure 21: Relation between reconstruction

methods & Diff. Unif.
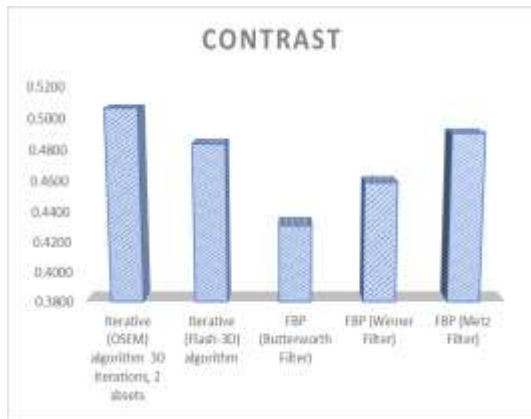
Figure 22: Relation between reconstruction methods & contrast.
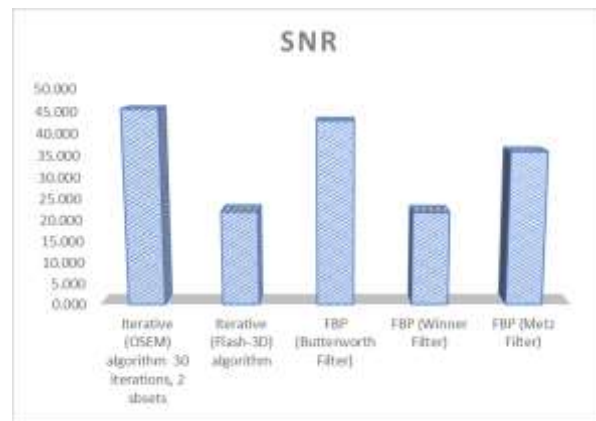
Figure 23: Relation between reconstruction methods & SNR.

Conclusion & Recommendations

Simultaneous DSPECT imaging is particularly desirable when two radiopharmaceuticals labeled with different isotopes bind to functionally different sites or display functions in different physiologic stages in the same anatomical area in patient. DSPECT acquisitions produce images that are in highly accurate spatial registration with each other. Therefore, the analytical errors due to different positions of the patient in two different scans can be minimized. Despite the above-mentioned advantages, DSPECT imaging approaches could potentially produce degraded and interfered images due to excess labeling of the second radioisotope. Close attention to several important factors is required to produce accurate images that reflect the distribution of each radionuclide.

The factors include acquisition and reconstruction parameters. In this study, we focused on the acquisition parameters, as source concentration, types of collimator and number of views, According to the results shown above in our study, the optimized parameters for the ^{99m}Tc /^{131}I dual isotope SPECT imaging are source concentration 20 mCi ^{99m}Tc-0.4 mCi ^{131}I (concentration ratio about 50-1), which resulted in a good correlation for the ration of consecration, with HEGP collimator and 64 number of views.

This study showed that, TPP can give the better quantification. The DSPECT image improvement increase with increasing the number of projections, but the DSPECT images still have good quality even with a small sampling number of projection data.

We conclude that the compensation for scattering is required to improve the dual SPECT image quality. The best way to perform such compensation is TEW subtraction method. Our experimental study showed the validity of the TEW method to elimination of the counts of the scattered photons in the DSPECT imaging. Since this approach is resistant to statistical noise and provides good estimation to the count of scattered photons, TEW is a practical method to use a SPECT study with dual-radioisotopes.

The study showed that, the reconstruction of DSPECT data were by (OSEM) iterative algorithm demonstrated quantitative accuracy comparable to FBP, FLASH-3D algorithm. However, in clinical practice, mainly in old systems, the FBP algorithm has several flaws: computationally faster, and an optimal filter has to be chosen to provide the best trade-off between image noise and image resolution for dual radionuclide. The difference between three types of filters of FBP algorithm, and their effect on DSPECT image quality was studied. We found that Metz Filter is more suitable than compared to other filters.

So, its recommended that to acquire a good quality DSPECT we must select ^{99m} Tc /^{131}I concentration ratio about 50-1, with HEGP collimator and 64 number of views. For scattering and reconstruction which required to improve the dual SPECT image quality, best way to perform such compensation is TEW subtraction method for scattering correction and OSEM iterative algorithm for reconstruction.

ACKNOWLEDGMENTS

References

[1].   Timmins R. "Dual isotope cross-talk correction in T c-99m /In-lll small-animal SPECT (2012) A thesis of master's degree of Science Carleton University, Canada.

[2].   Yang B.-H., Wang S-J, Shian J L. et all Physical phantom evaluation of simultaneous ^{99m}Tc /^{123}I SPECT imaging Nuclear Instruments and Methods in Physics Research A 652 (2011) 744–746

[3].   Devous, M.D., Payne, J.K., Lowe, J.L.: Dual isotope brain SPECT imaging with Technetium-99m and Iodine-123: clinical validation using Xenon-133 SPECT. J. Nucl. Med. 33 (1992) 1919-1924.

[4].   Schoeder, H., Topp, H., Friedrich, M., Jatzkewitz, A., Roser, M.: Thallium and indium antimyosin dual- isotope single-photon emission tomography in acute myocardial infarction to identify patients at further ischaemic risk. Eur. J. Nucl. Med. 21 (1994) 415-422

[5].   Bailey, D.L.: Transmission scanning in emission tomography. Eur. J. Nucl. Med. 25 (1998) 774-787

[6].   Links, J.M.: Simultaneous dual-radionuclide imaging: are the images trustworthy? Eur. J. Nucl. Med. 23 (1996) 1289-1291

[7].   Ivanovic, M., Weber, D.A., Loncaric, S., Franceschi, D.: Feasability of dual ra- dionuclide brain imaging with I-123 and Tc-99m. Med. Phys. 21 (1994) 667-674

[8].   CHANG C.J, HUANG W.S., SU K.H. et all Separation of two radionuclides in simultaneous dual-isotope imaging with independent component analysis Biomed Eng Appl Basis Comm, 2006(October); 18: 264-269

[9]. NAKAJIMA K., KAWANO M., KINAMI S.et all Dual-radionuclide simultaneous gastric emptying and bile transit study after gastric surgery with double-tract reconstruction Annals of Nuclear Medicine Vol. 19, No. 3, 185–191, 2005

[10]. Lowe V. J., Greer K. L., Hanson M.l W., et all Cardiac Phantom Evaluation of Simultaneously Acquired Dual-Isotope Rest Thallium-20 1/Stress Technetium-99m SPECT Images, The Journal of Nuclear Medicine vol. 34 No 11 November 1993

[11]. Kelty N. L., Holder L. E. and Khan S. H. Dual-Isotope Protocol for lndium-111 Capromab Pendetide Monoclonal Antibody Imaging J Nucl Med Techno.1998; 26:174-177

[12]. Yamada Y., MD, Nakano S., Gatate Y., et all Feasibility of simultaneous ^{99m}Tc-tetrofosmin and ^{123}I-BMIPP dual-tracer imaging with cadmium-zinc-telluride detectors in patients undergoing primary coronary intervention for acute myocardial infarction J Nucl Cardiol 2019

[13]. Powsner, R. A. & Powsner, E. R. (2008) .Essential nuclear medicine physics (2nd ed.) Wiley.

[14]. Cherry, S., Sorenson, J & ,.Phelps, M. (2012). Physics in nuclear medicine (4th ed.) Elsevier Health Sciences.

[15]. Agency, I. A. E. A& Bailey, D. L. (2015). Nuclear medicine physics: A handbook for teachers and students. Vienna: IAEA.

[16]. Tunninen, V., Kauppinen, T., & Eskola, H. (2017). Physical characteristics of collimators for dual-isotope imaging with ^{99m}Tc and ^{123}I.

[17]. Kobayashi M., Wakabayashi H • Kayano D. et all Application of a medium-energy collimator for I-131 imaging after ablation treatment of differentiated thyroid cancer Ann Nucl Med (2014) 28:551–558

[18]. King, M. A., et al. (2004). Chapter 22 - attenuation, scatter, and spatial resolution compensation in SPECT. (pp. 473-498) Elsevier Inc.

[19]. Hutton, B. F., Buvat, I., & Beekman, F. J. (2011). Review and current status of SPECT scatter correction. Physics in Medicine and Biology, 56(14), R85-R112.

[20]. Ogawa, K., Harata, Y., Ichihara, T., Kubo, A., & Hashimoto, S. (1991). A practical method for position- dependent Compton-scatter correction in single photon emission CT. IEEE Transactions on Medical Imaging, 10(3), 408-412.

[21]. Matsudaira, M., Nakajima, K., Tonami, N., & Hisada, K. (1997). Dual isotope SPECT with ^{99m}Tc and ^{123}I using four-energy-window (FEW) method. Kaku Igaku. the Japanese Journal of Nuclear Medicine, 34(11), 1013.

[22]. Kadrmas, D. J., Frey, E. C & Tsui, B. M. (1999). Simultaneous technetium-99m/thallium-201 SPECT imaging with model-based compensation for cross-contaminating effects. Physics in Medicine and Biology, 44(7), 1843-1860.

[23]. Tsui, B. M. W., Zhao, X., Frey, E. C., & McCartney, W. H. (1994). Quantitative single-photon emission computed tomography: Basic and clinical considerations. Seminars in Nuclear Medicine, 24(1), 38-65.

[24]. Cherry, S., Sorenson, J., & Phelps, M. (2012). Physics in nuclear medicine (4th ed.) Elsevier Health Sciences.

[25]. M. W. Groch and W. D. Erwin, "SPECT in the year 2000: basic principles," Journal of Nuclear Medicine Technology, vol. 28, no.4, pp. 233–244, 2000.

[26]. S. R. Cherry, J. A. Sorenson, and M. E. Phelps, Physics in Nuclear Medicine, Saunders, Philadelphia, Pa, USA, 3rd edition, 2003

[27]. P. P. Bruyant, "Analytic and iterative reconstruction algorithms in SPECT," Journal of Nuclear Medicine, vol. 45, no. 10, pp. 1343–1358, 2002.

[28]. Symbia Order No. A91MI-10410-1C-7600, USA, MI-1669.KF.WB.1500, c 06.2014, Siemens AG.